




## Chirality and correlations in the spontaneous spin-valley polarization of rhombohedral multilayer graphene


Yunsu Jang <sup>1,2</sup>, Youngju Park <sup>3</sup>, Jeil Jung,<sup>3,4,\*</sup> and Hongki Min <sup>1,2,†</sup>

<sup>1</sup>*Department of Physics and Astronomy, Seoul National University, Seoul 08826, Korea*

<sup>2</sup>*Center for Theoretical Physics, Seoul National University, Seoul 08826, Korea*

<sup>3</sup>*Department of Physics, University of Seoul, Seoul 02504, Korea*

<sup>4</sup>*Department of Smart Cities, University of Seoul, Seoul 02504, Korea*

 (Received 1 May 2023; revised 13 June 2023; accepted 14 June 2023; published 5 July 2023)

We investigate the total energies of spontaneous spin-valley polarized states in bi-, tri-, and tetralayer rhombohedral graphene where the long-range Coulomb correlations are accounted for within the random phase approximation. Our analysis of the phase diagrams for varying carrier doping and perpendicular electric fields shows that the exchange interaction between chiral electrons is the main driver of spin-valley polarization, while the presence of Coulomb correlations brings the flavor polarization phase boundaries to carrier densities close to the complete filling of the Mexican hat shape top at the Dirac points. We find that the tendency towards spontaneous spin-valley polarization is enhanced with the chirality of the bands and therefore with increasing number of layers.

DOI: [10.1103/PhysRevB.108.L041101](https://doi.org/10.1103/PhysRevB.108.L041101)

**Introduction.** Multilayer graphene has a unique stacking-dependent chiral structure [1–4], leading to a series of chiral two-dimensional electron systems (C2DESs) describable in terms of their sublattice and layer pseudospin degrees of freedom [5,6], which presents exciting opportunities for tailoring multilayer graphene’s electronic behavior through control of the stacking arrangement. The electron-electron interactions in multilayer graphene can give rise to a variety of phenomena [7–13]. In particular, rhombohedral multilayer graphene provides an excellent platform for studying interaction-induced phenomena as evidenced by recent experimental observations and theoretical studies of superconductivity and correlated phases [14–28] due to the flattening of its low-energy dispersion with increasing number of layers.

Here, we investigate the spontaneous spin-valley flavor polarization of rhombohedral multilayer graphene for finite carrier doping and perpendicular electric fields by calculating the polarization-dependent total energies including the exact exchange and long-range Coulomb correlations in the random phase approximation (RPA). In graphene, there are four distinct spin-valley flavors,  $(\uparrow, K)$ ,  $(\downarrow, K)$ ,  $(\uparrow, K')$ , and  $(\downarrow, K')$ . When electron-electron interactions are absent, these four flavors are occupied equally in the presence of carrier doping. However, electron-electron interactions can break this spin-valley population symmetry, resulting in electrons occupying only one or a subset of the available flavors [29], as shown in Fig. 1. While previous studies of flavor polarization have been carried out at the level of Hartree-Fock approximation [30,31], in this Research Letter we calculate the exchange-correlation energy including the Coulomb correlations within the RPA to

obtain the corresponding phase diagram of the spontaneous spin-valley polarization. Our findings reveal that the exchange interaction between chiral electrons is the driving force behind the emergence of spin-valley polarized states, while the Mexican hat band structure arising from the perpendicular electric field and the correlation effects jointly determine the transition point. The ground state is determined by comparing

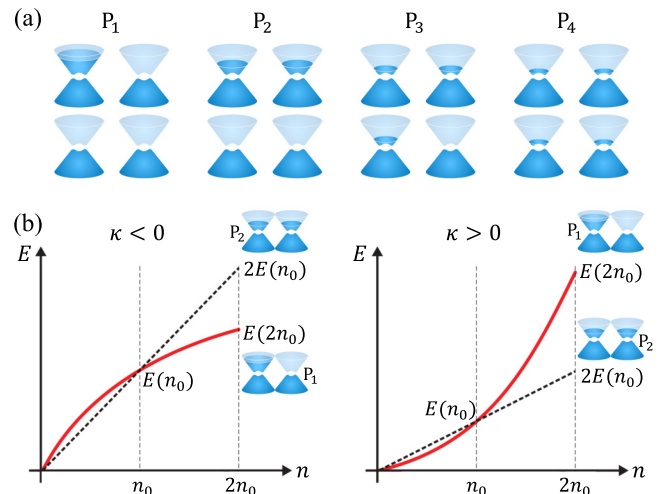


FIG. 1. (a) Schematic picture of the spin-valley polarized states  $P_1$ – $P_4$  that can result from any combination of  $K$  and  $K'$  valley and  $\uparrow$  and  $\downarrow$  spin polarizations. (b) Shape of the density dependence of the energy and the corresponding tendency toward spin-valley polarization. When the density dependence of the energy is concave down (up),  $E(2n_0) < 2E(n_0)$  [ $E(2n_0) > 2E(n_0)$ ] for a density  $n_0$  as in the left (right) panel; thus the system shows a tendency toward (against) spontaneous spin-valley polarization.

\*jeiljung@uos.ac.kr

†hmin@snu.ac.kr

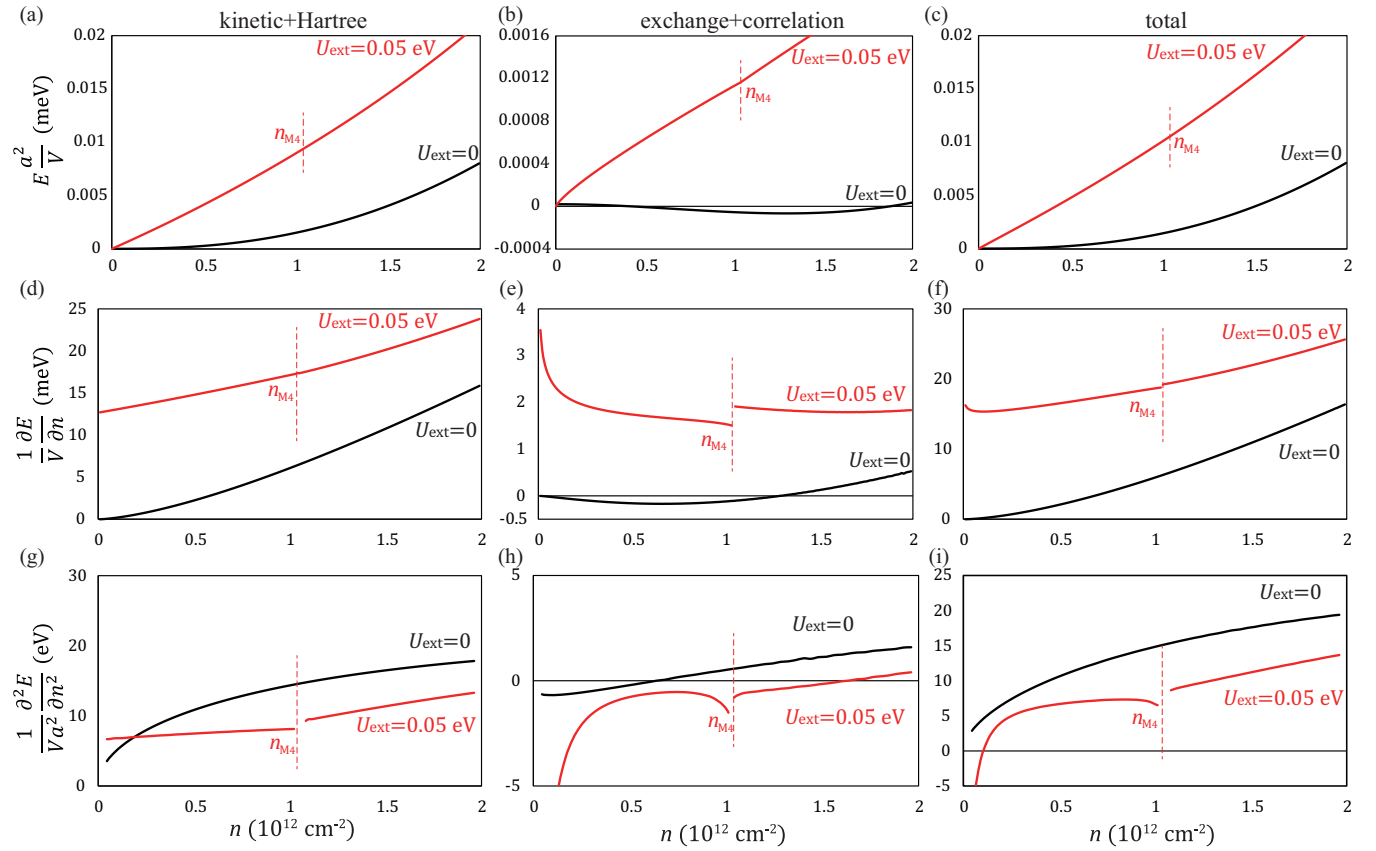


FIG. 2. Density dependence of (a) the kinetic plus Hartree energy, (b) the exchange plus correlation energy, (c) the total energy in ABC trilayer graphene for  $U_{\text{ext}} = 0$  (black) and  $U_{\text{ext}} = 0.05$  eV (red), (d), (e), and (f) their first derivatives, and (g), (h), and (i) their second derivatives with respect to the density. Note that the second derivatives are related to the electronic compressibility as  $\kappa^{-1} = n^2 \frac{\partial^2 E_{\text{tot}}}{\partial n^2}$ . The red vertical dashed lines represent the density  $n_{M_4} \approx 1.04 \times 10^{12} \text{ cm}^{-2}$  that fills the Mexican hat structure of the  $P_4$  state when  $U_{\text{ext}} = 0.05$  eV. For finite electric fields, the exchange-correlation energies show clearly negative compressibilities up to densities above  $n_{M_4}$ , while the instability from total energies is expected at low densities near the band edges. Here, we use the effective fine structure constant  $\alpha = \frac{e^2}{\epsilon \hbar v} = 1$ , where  $\epsilon$  is the effective dielectric constant.

the total energies corresponding to phases  $P_1$ – $P_4$ , and we will later discuss different possible intermediate mixed states with unequal flavor concentrations in the Discussion section. The general tendency towards (against) spontaneous flavor polarization can be predicted from the density dependence of its energy as concave down (up) as depicted in Fig. 1(b) where the system will tend towards (against) spontaneous spin-valley flavor polarization. The electronic compressibility is therefore closely connected to spontaneous flavor polarization and can serve as a powerful thermodynamic probe of the electron-electron interaction effect. The inverse electronic compressibility can be expressed as  $\kappa^{-1} = n^2 \partial \mu / \partial n$ , where  $n$  is the carrier density,  $\mu = \partial E_{\text{tot}} / \partial N$  is the chemical potential,  $E_{\text{tot}}$  is the total ground-state energy, and  $N$  is the total number of particles in the system.

*Density dependence of the energies and their derivatives.* To calculate the ground-state energy, we consider the contributions from the kinetic, Hartree, exchange, and correlation energies. In the presence of a perpendicular electric field  $E_{\text{ext}}$ , we start by obtaining a mean-field band structure that takes into account the effect of the self-consistent Hartree potential, as well as the energy gap opening due to  $E_{\text{ext}}$ . Next, we compute the exchange-correlation energy by using the

integration-over-coupling-constant method within the RPA. Further details regarding the derivation can be found in the Supplemental Material [32]. Figure 2 shows the density dependence of the kinetic plus Hartree energy, the exchange plus correlation energy, the total energy, and their first and second derivatives with respect to the density in ABC-stacked trilayer graphene for  $U_{\text{ext}} = 0$  and  $U_{\text{ext}} = 0.05$  eV, respectively, where  $U_{\text{ext}} = eE_{\text{ext}}d$  with the interlayer separation  $d = 3.35$  Å.

First, let us consider the  $U_{\text{ext}} = 0$  case. In our calculations, we used the full bands continuum Hamiltonian, but here our discussion is based on the low-energy C2DES model of rhombohedral multilayer graphene with chirality index  $J$  which coincides with layer number [5,6]:

$$\mathcal{H}_J(\mathbf{k}) = t_{\perp} \begin{pmatrix} 0 & (\frac{\hbar v_{\perp}}{t_{\perp}})^J \\ (\frac{\hbar v_{\perp}}{t_{\perp}})^J & 0 \end{pmatrix}, \quad (1)$$

where  $k_{\pm} = k_x \pm ik_y$ ,  $v$  is the in-plane Fermi velocity of monolayer graphene, and  $t_{\perp}$  is the nearest-neighbor interlayer hopping. The eigenenergies of Eq. (1) are given by  $\epsilon_{s,k} = st_{\perp}(\hbar v|k|/t_{\perp})^J$  with  $s = \pm 1$  for positive and negative energy states, respectively. For  $U_{\text{ext}} = 0$ , the Hartree energy is zero,

and the kinetic energy per particle is given by  $\frac{E_{\text{kin}}}{N} = \frac{2}{J+2}\varepsilon_F$ , where  $\varepsilon_F$  is the Fermi energy. Since  $\varepsilon_F \sim k_F^J$  and  $n \sim k_F^2$ , where  $k_F$  is the Fermi wave vector, we have  $E_{\text{kin}} \sim k_F^{J+2} \sim n^{\frac{J+2}{2}}$ , which is concave up with respect to the density  $n$ . Therefore the kinetic energy does not favor spin-valley flavor polarization. In contrast, the exchange energy per particle is given by  $\frac{E_{\text{ex}}}{N} = C_1 \frac{e^2}{\epsilon_0} k_F$ , where  $C_1$  is a coefficient with weak density dependence such that  $C_1 < 0$  for  $J \geq 2$  ( $C_1 > 0$  for  $J = 1$ ) due to the dominant intraband (interband) exchange interaction [36]. This means that for  $J \geq 2$ ,  $E_{\text{ex}} \sim -k_F^3 \sim -n^{\frac{3}{2}}$ , which is concave down with respect to  $n$ , and thus the exchange energy favors flavor polarization. From the power-law dependence, we find that at small carrier densities, the exchange energy is dominant over the kinetic energy, and there is a tendency toward flavor polarization. However, at sufficiently large densities, the kinetic energy becomes dominant over the exchange energy, and there is a tendency toward the normal phase. When correlation effects are included, the tendency toward flavor polarization is reduced due to the concave-up dependence of the correlation energy on density. The exchange contribution to the electronic compressibility is negative, but when all contributions are combined, the electronic compressibility remains positive. Thus ABC trilayer graphene remains in the normal phase for  $U_{\text{ext}} = 0$ , as indicated by the black line in Fig. 2(i).

This scenario changes when  $U_{\text{ext}} \neq 0$ , where the system develops a characteristic ‘‘Mexican hat’’ structure that we obtain self-consistently by considering the kinetic and Hartree contributions. As the density  $n$  increases, the Fermi energy also increases, causing the Fermi surface to evolve from a disk with a concentric hole to a fully filled disk. In our approximation, the Fermi energy corresponds to the first derivative of the kinetic plus Hartree energy with respect to  $n$ ; so the second derivative of the energy remains positive even in the presence of  $U_{\text{ext}}$ , indicating a tendency toward the normal phase. The exchange energy is also influenced by a finite  $U_{\text{ext}}$ . A perpendicular electric field causes some pseudospins in the conduction and valence bands to align oppositely along the  $z$  direction. This alignment results in an increase of the interband contribution to the exchange energy with increasing density, up to a certain density where the oppositely aligned pseudospins induce a maximum exchange energy. Beyond this density, the intraband contribution to the exchange energy dominates, causing the exchange contribution to decrease with increasing density, similar to the  $U_{\text{ext}} = 0$  case. Additionally, as the pseudospins in the conduction band become more aligned along the same direction due to the external field, the second derivative of the exchange energy becomes more negative, making the exchange energy more concave down and enhancing the tendency toward spin-valley polarization. When the density  $n$  crosses the density  $n_M$  that fills the Mexican hat structure, the negative intraband exchange contribution from electrons near  $\mathbf{k} = 0$  becomes absent, resulting in a less negative contribution to the exchange energy. This causes a jump in the first derivative of the exchange energy, as shown in Fig. 2(e). We note that typically the correlation reduces the exchange effects. At low densities, the electronic compressibility  $\kappa$  of the system becomes negative for  $U_{\text{ext}} \neq 0$ , which means that the system no longer remains

in the normal phase and instead enters a flavor polarized state. However, at high enough densities, the kinetic energy associated with large  $\mathbf{k}$  becomes dominant, transitioning back to the normal phase.

*Phase diagram of multilayer graphene.* The density-dependent total energy analysis shows an inherent tendency of the exchange interaction towards spin-valley flavor polarization. In the following we present the flavor polarization phase diagram of bilayer, trilayer, and tetralayer rhombohedral multilayer graphene as a function of carrier density  $n$  and external potential  $U_{\text{ext}}$ , where the total energies include the RPA correlations. To calculate the exchange-correlation energy in multilayer graphene, we use the rotational transformation of the chiral wave function to obtain the chiral wave function at any angle from the wave function obtained at a given angle, greatly facilitating the calculations [36]. Figures 3(a)–3(c) show the phase diagrams of AB, ABC, and ABCA stacked multilayer graphene as a function of  $n$  and  $U_{\text{ext}}$ . To further understand these phase diagrams, let us examine the band structure change of ABC trilayer graphene near the phase boundaries along the white dashed line in Fig. 3(b) when we use a fixed  $U_{\text{ext}} = 0.05$  eV. For example, the band fillings for the  $P_3$  and  $P_4$  states near the phase boundaries have qualitatively different characters. For a given equal density in the  $P_3$  state, the Mexican hat band structure is fully filled beyond the top of the hat near the Dirac points  $K^{(\prime)}$ , while for the  $P_4$  state the electrons fill up to lower energies. Because in the  $P_3$  phase the (negative intraband) exchange contribution from electrons near  $\mathbf{k} = 0$  is already filled, an increase in the carrier density results in a less negative contribution to the exchange energy compared with the  $P_4$  phase, where the electrons are mainly filling the ring-shaped band edges and the exchange energy gain is greater [see the insets in Fig. 3(d)]. This implies that in practice there will be a flavor polarization transition just after the Mexican hat structure is completely filled because the exchange-driven flavor polarization is partly countered by the Coulomb-correlation-driven screening. The energy difference  $E_{34}$  between the  $P_3$  and  $P_4$  states becomes positive after the critical density  $n_c^{34}$  as indicated by the black arrow in Fig. 3(d). As the perpendicular field is increased to  $U_{\text{ext}} = 0.1$  eV [see Fig. 3(e)], the density required to fill the Mexican hat structure ( $n_{M_3}$ ) and the phase transition critical density ( $n_c^{34}$ ) also increase. In the higher-density region, the difference between the two densities  $n_{M_3}$  and  $n_c^{34}$  becomes smaller since the kinetic plus Hartree energy is dominant over the exchange-correlation energy. Thus  $n_{M_3}$  and  $n_c^{34}$  eventually merge at the same point, showing a kink structure in the phase diagram. For a sufficiently high  $U_{\text{ext}}$  above the kink point, the Mexican hat structures of both the  $P_3$  state and the  $P_4$  state are partially filled, and  $E_{34}$  increases by  $U_{\text{ext}}$  as shown in Fig. 3(e), resulting in a decreased  $n_c^{34}$ . The other phase boundaries in the phase diagram can be discussed using similar arguments.

*Discussion.* The calculated phase diagram in Fig. 3 captures the main features of the carrier density and electric field dependence of the spontaneous spin-valley polarization recently observed in rhombohedral trilayer graphene [14] and bilayer graphene [16]. The explicit inclusion of the RPA correlations allows us to achieve agreement with experiments with a conventional value of the dielectric constant of  $\epsilon_r \approx 2.6$  corresponding to the effective interaction strength  $\alpha = 1$ , rather

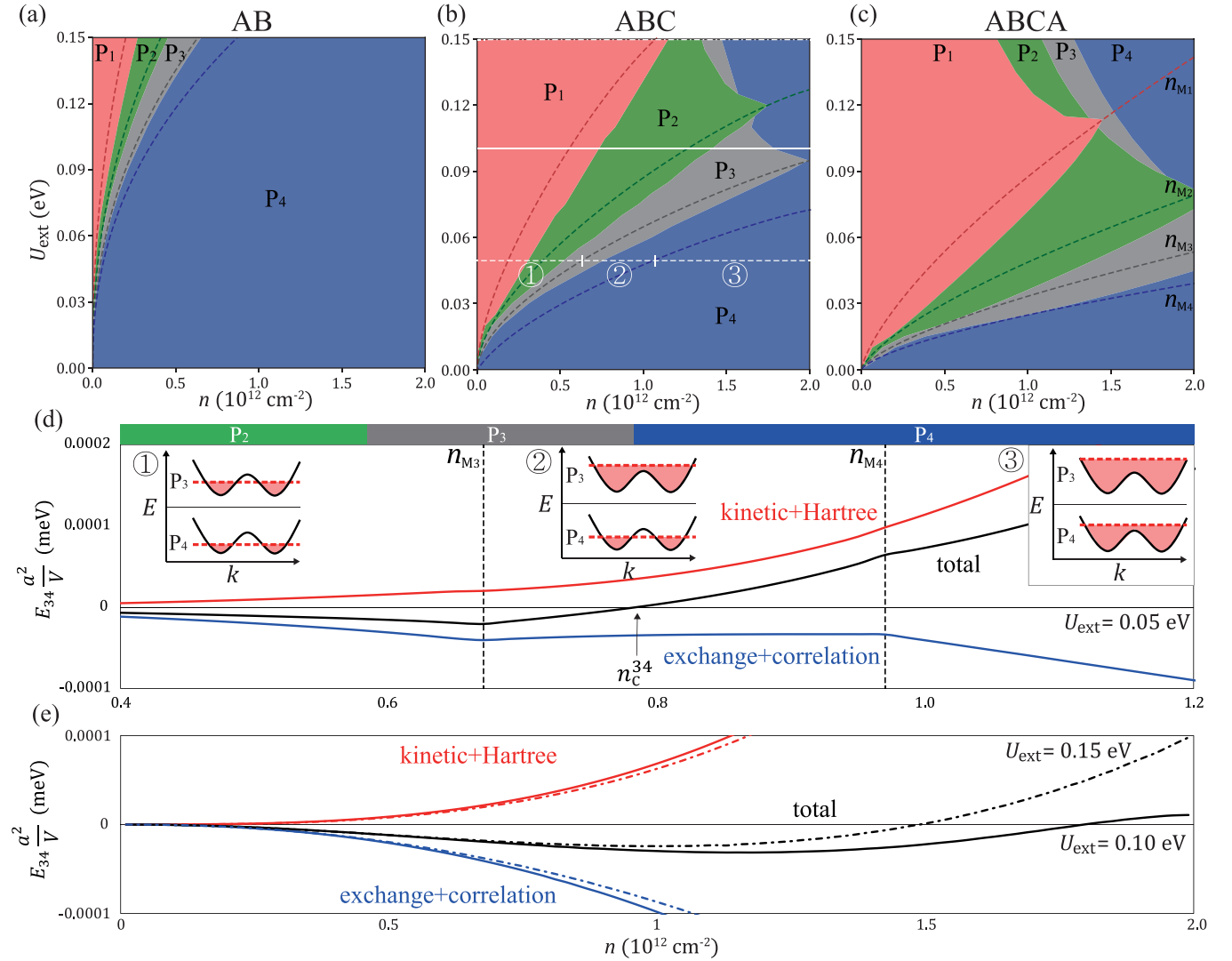


FIG. 3. Phase diagrams of (a) AB, (b) ABC, and (c) ABCA stacked multilayer graphene. (d) and (e) Energy difference between the  $P_3$  and  $P_4$  states for ABC trilayer graphene for (d)  $U_{\text{ext}} = 0.05$  eV following the white dashed line in (b), and (e)  $U_{\text{ext}} = 0.1$  eV (solid lines) and  $U_{\text{ext}} = 0.15$  eV (dash-dotted lines) following the white solid and dash-dotted lines in (b), respectively. The insets in (d) show the low-energy conduction band and the Fermi energy of the occupied flavors for the  $P_3$  and  $P_4$  states in regions ①, ②, and ③ in (b). In (d), these regions are separated by the vertical dashed lines at  $n = n_{M3}$  and  $n = n_{M4}$  that fill the Mexican hat structure of the  $P_3$  and  $P_4$  states, respectively, when  $U_{\text{ext}} = 0.05$  eV. Here, we use  $\alpha = 1$ .

than using unrealistic screening constants to compensate the overestimation of the exchange interaction. Instead, in our calculation the Coulomb correlations cause the phase boundaries to appear close to the densities where the top of the Mexican hat is filled completely for a given flavor polarization. Our theory is expected to be valid in the limit of strong electric fields and large densities, showing that the phase boundary slopes agree closely with experiments in this regime.

So far, our analysis has been based on pure flavor polarized states rather than intermediate mixed states with unequal flavor concentrations. Further discussion of the mixed states can be found in the Supplemental Material [32]. Below, we discuss some details left out in our study. Firstly, our work assumes an isotropic circular symmetry around the Dirac points neglecting the trigonal warping of the bands to reduce the computational load. These effects are expected to be small

away from  $n = 0$  and  $U_{\text{ext}} = 0$ , thus allowing us to capture the spontaneous spin-valley polarized phases that are manifested away from this limit. Secondly, our current calculation does not include any anisotropy term that favors a certain flavor polarization over another. The absence of a flavor anisotropy term may also explain the appearance of the  $P_3$  state in our current calculations, which is absent in experiments. We leave the analysis of flavor degeneracy breaking as an open question for future research.

In summary, we have discussed the spin-valley flavor polarization in bi-, tri-, and tetralayer rhombohedral graphene in light of the long-range Coulomb correlations neglected in the literature. We have shown that while the exchange interaction together with the chiral bands drives the instability towards flavor polarization, the screening due to Coulomb correlations brings the phase boundary points to lie close to the carrier densities that fill the top of the Mexican hat band structure.



The carrier density, external electric field, and band chirality influence the phase diagram of the spin-valley flavor polarized states in rhombohedral multilayer graphene, suggesting a greater tendency of flavor polarization in systems with larger band chirality and, therefore, a larger number of layers.

*Acknowledgments.* This work was supported by the National Research Foundation of Korea (NRF) grants funded by the Korea government (MSIT) (Grants No. 2018R1A2B6007837 and No. 2023R1A2C1005996) and the

Creative-Pioneering Researchers Program through Seoul National University (SNU). Y.P. acknowledges support from Samsung Science and Technology Foundation Grant No. SSTF-BA1802-06. J.J. acknowledges support from NRF (Grant No. 2020R1A2C3009142), KISTI (Grant No. KSC-2022-CRE-0514), the resources of Urban Big data and AI Institute (UBAI) at UOS, and the Korean Ministry of Land, Infrastructure and Transport (MOLIT) from the Innovative Talent Education Program for Smart Cities.

- 
- [1] A. H. Castro Neto, F. Guinea, N. M. R. Peres, K. S. Novoselov, and A. K. Geim, The electronic properties of graphene, *Rev. Mod. Phys.* **81**, 109 (2009).
- [2] S. Das Sarma, S. Adam, E. H. Hwang, and E. Rossi, Electronic transport in two-dimensional graphene, *Rev. Mod. Phys.* **83**, 407 (2011).
- [3] D. N. Basov, M. M. Fogler, A. Lanzara, F. Wang, and Y. Zhang, Colloquium: Graphene spectroscopy, *Rev. Mod. Phys.* **86**, 959 (2014).
- [4] *Graphene Nanoelectronics*, edited by H. Raza (Springer, New York, 2012).
- [5] H. Min and A. H. MacDonald, Chiral decomposition in the electronic structure of graphene multilayers, *Phys. Rev. B* **77**, 155416 (2008).
- [6] H. Min and A. H. MacDonald, Electronic structure of multilayer graphene, *Prog. Theor. Phys. Suppl.* **176**, 227 (2008).
- [7] H. Min, G. Borghi, M. Polini, and A. H. MacDonald, Pseudospin magnetism in graphene, *Phys. Rev. B* **77**, 041407(R) (2008).
- [8] J. Jung and A. H. MacDonald, Gapped broken symmetry states in ABC-stacked trilayer graphene, *Phys. Rev. B* **88**, 075408 (2013).
- [9] J. Martin, B. E. Feldman, R. T. Weitz, M. T. Allen, and A. Yacoby, Local Compressibility Measurements of Correlated States in Suspended Bilayer Graphene, *Phys. Rev. Lett.* **105**, 256806 (2010).
- [10] R. T. Weitz, M. T. Allen, B. E. Feldman, J. Martin, and A. Yacoby, Broken-symmetry states in doubly gated suspended bilayer graphene, *Science* **330**, 812 (2010).
- [11] A. L. Grushina, D. K. Ki, M. Koshino, A. A. L. Nicolet, C. Faugeras, E. McCann, M. Potemski, and A. Morpurgo, Insulating state in tetralayers reveals an even-odd interaction effect in multilayer graphene, *Nat. Commun.* **6**, 6419 (2015).
- [12] Y. Nam, D. Ki, M. Koshino, E. McCann, and A. Morpurgo, Interaction-induced insulating state in thick multilayer graphene, *2D Mater.* **3**, 045014 (2016).
- [13] C. Yoon, Y. Jang, J. Jung, and H. Min, Broken sublattice symmetry states in Bernal stacked multilayer graphene, *2D Mater.* **4**, 021025 (2017).
- [14] H. Zhou, T. Xie, A. Ghazaryan, T. Holder, J. R. Ehrets, E. M. Spanton, T. Taniguchi, K. Watanabe, E. Berg, M. Serbyn, and A. F. Young, Half- and quarter-metals in rhombohedral trilayer graphene, *Nature (London)* **598**, 429 (2021).
- [15] H. Zhou, T. Xie, T. Taniguchi, K. Watanabe, and A. F. Young, Superconductivity in rhombohedral trilayer graphene, *Nature (London)* **598**, 434 (2021).
- [16] H. Zhou, L. Holleis, Y. Saito, L. Cohen, W. Huynh, C. L. Patterson, F. Yang, T. Taniguchi, K. Watanabe, and A. F. Young, Isospin magnetism and spin-polarized superconductivity in Bernal bilayer graphene, *Science* **375**, 774 (2022).
- [17] A. M. Seiler, F. R. Geisenhof, F. Winterer, K. Watanabe, T. Taniguchi, T. Xu, F. Zhang, and R. T. Weitz, Quantum cascade of correlated phases in trigonally warped bilayer graphene, *Nature (London)* **608**, 298 (2022).
- [18] S. C. de la Barrera, S. Aronson, Z. Zheng, K. Watanabe, T. Taniguchi, Q. Ma, P. Jarillo-Herrero, and R. Ashoori, Cascade of isospin phase transitions in Bernal-stacked bilayer graphene at zero magnetic field, *Nat. Phys.* **18**, 771 (2022).
- [19] A. L. Szabó and B. Roy, Metals, fractional metals, and superconductivity in rhombohedral trilayer graphene, *Phys. Rev. B* **105**, L081407 (2022).
- [20] D.-C. Lu, T. Wang, S. Chatterjee, and Y.-Z. You, Correlated metals and unconventional superconductivity in rhombohedral trilayer graphene: A renormalization group analysis, *Phys. Rev. B* **106**, 155115 (2022).
- [21] F. R. Geisenhof, F. Winterer, A. M. Seiler, J. Lenz, F. Zhang, and R. T. Weitz, Impact of electric field disorder on broken-symmetry states in ultraclean bilayer graphene, *Nano Lett.* **22**, 7378 (2022).
- [22] A. Ghazaryan, T. Holder, E. Berg, and M. Serbyn, Multilayer graphenes as a platform for interaction-driven physics and topological superconductivity, *Phys. Rev. B* **107**, 104502 (2023).
- [23] A. Jimeno-Pozo, H. Sainz-Cruz, T. Cea, P. Pantaleón, and F. Guinea, Superconductivity from electronic interactions and spin-orbit enhancement in bilayer and trilayer graphene, *Phys. Rev. B* **107**, L161106 (2023).
- [24] W. Qin, C. Huang, T. Wolf, N. Wei, I. Blinov, and A. MacDonald, Functional Renormalization Group Study of Superconductivity in Rhombohedral Trilayer Graphene, *Phys. Rev. Lett.* **130**, 146001 (2023).
- [25] A. Patri and T. Senthil, Strong correlations in ABC-stacked trilayer graphene: Moiré is important, *Phys. Rev. B* **107**, 165122 (2023).
- [26] Z. Dong, M. Davydova, O. Ogunnaike, and L. Levitov, Isospin and momentum-polarized orders in bilayer graphene, *Phys. Rev. B* **107**, 075108 (2023).
- [27] J.-X. Lin, Y. Wang, N. J. Zhang, K. Watanabe, T. Taniguchi, L. Fu, and J. Li, Spontaneous momentum polarization and diodicity in Bernal bilayer graphene, [arXiv:2302.04261](https://arxiv.org/abs/2302.04261).
- [28] G. Shavit and Y. Oreg, Inducing superconductivity in bilayer graphene by alleviation of the Stoner blockade, [arXiv:2303.04176](https://arxiv.org/abs/2303.04176).
- [29] J. Jung, M. Polini, and A. H. MacDonald, Persistent current states in bilayer graphene, *Phys. Rev. B* **91**, 155423 (2015).

- [30] C. Huang, T. Wolf, W. Qin, N. Wei, I. Blinov, and A. H. MacDonald, Spin and orbital metallic magnetism in rhombohedral trilayer graphene, *Phys. Rev. B* **107**, L121405 (2023).
- [31] M. Xie and S. Das Sarma, Flavor symmetry breaking in spin-orbit coupled bilayer graphene, *Phys. Rev. B* **107**, L201119 (2023).
- [32] See Supplemental Material at <http://link.aps.org/supplemental/10.1103/PhysRevB.108.L041101> for the detailed derivations of the exchange-correlation energy using a self-consistent Hartree band structure and intermediate mixed states in the phase diagram. The Supplemental Material also contains Refs. [33–35].
- [33] J. Jang, S. Ahn, and H. Min, Optical conductivity of black phosphorus with a tunable electronic structure, *2D Mater.* **6**, 025029 (2019).
- [34] G. F. Giuliani and G. Vignale, *Quantum Theory of the Electron Liquid* (Cambridge University Press, Cambridge, 2005).
- [35] M. Polini, R. Asgari, Y. Barlas, T. Pereg-Barnea, and A. H. MacDonald, Graphene: A pseudochiral Fermi liquid, *Solid State Commun.* **143**, 58 (2007).
- [36] Y. Jang, E. H. Hwang, A. H. MacDonald, and H. Min, Stacking dependence of carrier interactions in multilayer graphene systems, *Phys. Rev. B* **92**, 041411(R) (2015).